

---

# BANDWIDTH SELECTION FOR GAUSSIAN KERNEL RIDGE REGRESSION VIA JACOBIAN CONTROL

---

**Oskar Allerbo**

Mathematical Sciences  
University of Gothenburg and Chalmers University of Technology  
allerbo@chalmers.se

**Rebecka Jörnsten**

Mathematical Sciences  
University of Gothenburg and Chalmers University of Technology  
jornsten@chalmers.se

## ABSTRACT

Most machine learning methods require tuning of hyper-parameters. For kernel ridge regression with the Gaussian kernel, the hyper-parameter is the bandwidth. The bandwidth specifies the length scale of the kernel and has to be carefully selected to obtain a model with good generalization. The default methods for bandwidth selection, cross-validation and marginal likelihood maximization, often yield good results, albeit at high computational costs. Inspired by Jacobian regularization, we formulate an approximate expression for how the derivatives of the functions inferred by kernel ridge regression with the Gaussian kernel depend on the kernel bandwidth. We use this expression to propose a closed-form, computationally feather-light, bandwidth selection heuristic, based on controlling the Jacobian. In addition, the Jacobian expression illuminates how the bandwidth selection is a trade-off between the smoothness of the inferred function and the conditioning of the training data kernel matrix. We show on real and synthetic data that compared to cross-validation and marginal likelihood maximization, our method is on par in terms of model performance, but up to six orders of magnitude faster.

**Keywords:** Kernel Ridge Regression, Bandwidth Selection, Jacobian Regularization

## 1 Introduction

Kernel ridge regression, KRR, is a non-linear, closed-form solution regression technique used within a wide range of applications (Zahrt et al., 2019; Ali et al., 2020; Chen and Leclair, 2021; Fan et al., 2021; Le et al., 2021; Safari and Rahimzadeh Arashloo, 2021; Shahsavar et al., 2021; Singh Alvarado et al., 2021; Wu et al., 2021; Chen et al., 2022). It is related to Gaussian process regression (Krige, 1951; Matheron, 1963; Williams and Rasmussen, 2006), but with a frequentist, rather than a Bayesian, perspective. Apart from being useful on its own merits, in recent years, the similarities between KRR and neural networks have been highlighted, making the former an increasingly popular tool for gaining better theoretical understandings of the latter (Belkin et al., 2018; Jacot et al., 2018; Chen and Xu, 2020; Geifman et al., 2020; Ghorbani et al., 2020, 2021; Mei et al., 2021).

However, kernelization introduces hyper-parameters, which need to be carefully tuned in order to obtain good generalization. The bandwidth,  $\sigma$ , is a hyper-parameter used by many kernels, including the Gaussian, or radial basis function, kernel. The bandwidth specifies the length scale of the kernel. A kernel with a too small bandwidth will treat most new data as far from any training observation, while a kernel with a too large bandwidth will treat each new data point as basically equidistant to all training observations. None of these situations will result in good generalization.

The problem of bandwidth selection has been extensively studied for kernel density estimation, KDE, which is the basis for KDE-based kernel regression, such as the Nadaraya-Watson estimator (Nadaraya, 1964; Watson, 1964) and

locally weighted regression (Cleveland and Devlin, 1988). Köhler et al. (2014) review existing methods for bandwidth selection for KDE-based kernel regression, methods that all make varying strong assumptions on the underlying data density and smoothness of the non-parametric regression model, and how the latter can be approximately estimated. On one end of the spectrum, cross-validation and marginal likelihood maximization make almost no assumptions on the underlying data structure, resulting in very flexible, but computationally heavy, estimators, with high variance. On the other end, with strong assumptions on the underlying data structure, Silverman’s rule of thumb, originally from 1986, (Silverman, 2018) is a computationally light estimator with low variance, but possibly far from optimal. Other approaches on the spectrum include Park and Marron (1990), Sheather and Jones (1991), and Fan and Gijbels (1995).

Although similar in name and usage, KRR and KDE-based kernel regression are not the same. While KDE-based kernel regression estimates the probability density of the data, and uses this density to estimate  $\mathbb{E}(y|\mathbf{x})$ , KRR takes a functional perspective, directly estimating  $\hat{y} = \hat{f}(\mathbf{x})$ , similarly to how is done in neural networks.

For neural networks, Jacobian regularization, which penalizes the Frobenius norm of the Jacobian,  $\left\| \frac{\partial \hat{f}(\mathbf{x})}{\partial \mathbf{x}} \right\|_F^2$ , has recently been successfully applied to improve generalization (Jakubovitz and Giryes, 2018; Chan et al., 2019; Hoffman et al., 2019; Finlay et al., 2020; Bai et al., 2021). The Jacobian penalty is a non-linear generalization of the linear ridge penalty. To see this, consider the linear model  $\hat{f}(\mathbf{x}) = \mathbf{x}^\top \boldsymbol{\beta}$ , for which the Jacobian penalty becomes exactly the ridge penalty,  $\|\boldsymbol{\beta}\|_2^2$ . Thus, both Jacobian and ridge regularization improve generalization by constraining the derivatives of the inferred function.

This connection motivates our investigation into how Jacobian constraints can be applied for bandwidth selection in KRR: If we knew how the kernel bandwidth affects the Jacobian of the inferred function, then we could use Jacobian control as a criterion for selecting the bandwidth.

Our main contributions are:

- We derive an approximate expression for the Jacobian of the function inferred by KRR with the Gaussian kernel.
- We propose a closed-form, computationally feather-light, bandwidth selection method for KRR with the Gaussian kernel, based on controlling the approximate Jacobian.
- We show on synthetic and real data that Jacobian-based bandwidth selection outperforms cross-validation and marginal likelihood maximization in terms of computation speed, and Silverman’s method in terms of model performance.

## 2 Bandwidth Selection through Jacobian Control

Consider the left panel of Figure 1. When large (absolute) derivatives of the inferred function are allowed, the function varies more rapidly between observations, while a function with constrained derivatives varies more smoothly, which intuitively improves generalization. However, the derivatives must not be too small as this leads to an overly smooth estimate, as seen in the right panel.

The functions in Figure 1 are all constructed using kernel ridge regression, KRR, with the Gaussian kernel. For training data  $\mathbf{X} \in \mathbb{R}^{n \times p}$  and  $\mathbf{y} \in \mathbb{R}^n$ , the objective function of KRR is

$$\min_{f \in \mathcal{H}_k} \left\| \mathbf{y} - [f(\mathbf{x}_1) \ \dots \ f(\mathbf{x}_n)]^\top \right\|_2^2 + \lambda \|f\|_{\mathcal{H}_k}^2. \quad (1)$$

$\mathcal{H}_k$  denotes the reproducing kernel Hilbert space corresponding to the symmetric, positive semi-definite kernel function  $k(\mathbf{x}, \mathbf{x}')$ , and  $\lambda \geq 0$  is the regularization strength. Solving Equation 1, a prediction  $\hat{f}(\mathbf{x}^*) \in \mathbb{R}$ , where  $\mathbf{x}^* \in \mathbb{R}^p$ , is given by

$$\hat{f}(\mathbf{x}^*) = \mathbf{k}(\mathbf{x}^*, \mathbf{X})^\top \cdot (\mathbf{K}(\mathbf{X}, \mathbf{X}) + \lambda \mathbf{I})^{-1} \cdot \mathbf{y}, \quad (2)$$

where  $\mathbf{k}(\mathbf{x}^*, \mathbf{X}) \in \mathbb{R}^n$  and  $\mathbf{K}(\mathbf{X}, \mathbf{X}) \in \mathbb{R}^{n \times n}$  are two kernel matrices,  $\mathbf{k}(\mathbf{x}^*, \mathbf{X})_i = k(\mathbf{x}^*, \mathbf{x}_i)$  and  $\mathbf{K}(\mathbf{X}, \mathbf{X})_{ij} = k(\mathbf{x}_i, \mathbf{x}_j)$ .

The Gaussian kernel is given by

$$k_G(\mathbf{x}, \mathbf{x}', \sigma) := \exp \left( -\frac{\|\mathbf{x} - \mathbf{x}'\|_2^2}{2\sigma^2} \right), \quad (3)$$

where the bandwidth,  $\sigma$ , specifies the length-scale of the kernel, i.e. what is to be considered as “close”.

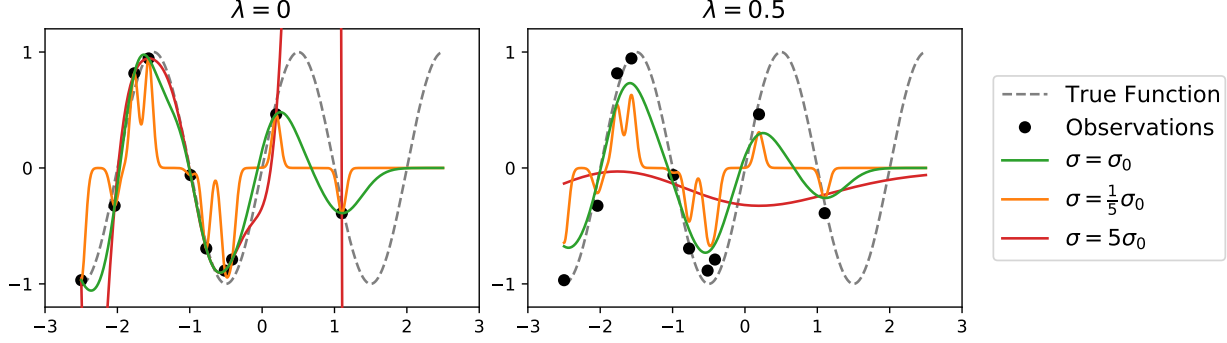


Figure 1: Kernel ridge regression with different bandwidths and different regularizations, where  $\sigma_0$  is the bandwidth proposed by the Jacobian method, and  $\lambda$  is the strength of the regularization. In the absence of regularization, regardless of the bandwidth, the inferred function perfectly interpolates the training data, i.e. it hits all training observations. When the bandwidth is too small, the kernel considers most new observations as far away from any training data and quickly resorts to its default value, 0. A too large bandwidth, on the other hand, results in extreme predictions between some of the observations. The addition of regularization affects larger bandwidths more than smaller ones. A too large bandwidth, in combination with regularization, produces a function that is too simple to capture the patterns in the training data.

Returning to our aspiration from above, we would like to select  $\sigma$  in Equation 3 to control  $\left\| \frac{\partial \hat{f}(\mathbf{x}^*)}{\partial \mathbf{x}^*} \right\|_F = \left\| \frac{\partial \hat{f}(\mathbf{x}^*)}{\partial \mathbf{x}^*} \right\|_2$ , with  $\hat{f}(\mathbf{x}^*)$  given by Equation 2.

In general, there is no simple expression for  $\left\| \frac{\partial \hat{f}(\mathbf{x}^*)}{\partial \mathbf{x}^*} \right\|_2$ , but in Definition 1, we state an approximation that is based on derivations that we will present in Section 2.1.

**Definition 1** (Approximate Jacobian Norm).

$$J_2^a(\sigma) = J_2^a(\sigma, l_{\max}, n, p, \lambda) := \frac{1}{\sigma} \cdot \frac{1}{n \cdot \exp \left( - \left( \frac{((n-1)^{1/p} - 1) \pi \sigma}{2l_{\max}} \right)^2 \right) + \lambda} \cdot C(n, \|\mathbf{y}\|_2), \quad (4)$$

where  $l_{\max}$  denotes the maximum distance between two training observations, and  $C(n, \|\mathbf{y}\|_2)$  is a constant with respect to  $\sigma$ .

**Remark 1:** Since we are only interested in how  $J_2^a$  depends on  $\sigma$ , we will henceforth, with a slight abuse of notation, omit the constant  $C(n, \|\mathbf{y}\|_2)$ .

**Remark 2:** Technically, since we use a univariate response,  $\frac{\partial \hat{f}(\mathbf{x}^*)}{\partial \mathbf{x}^*}$  is a special case of the Jacobian, the gradient. We chose, however, to use the word Jacobian, since nothing in our derivations restricts us to the univariate case.

**Remark 3:** We will refer to the two  $\sigma$  dependent factors in Equation 4 as

$$j_a(\sigma) := \frac{1}{\sigma} \quad \text{and} \quad j_b(\sigma) := \frac{1}{n \cdot \exp \left( - \left( \frac{((n-1)^{1/p} - 1) \pi \sigma}{2l_{\max}} \right)^2 \right) + \lambda}. \quad (5)$$

Proposition 1 below characterizes how the approximate Jacobian norm,  $J_2^a$ , depends on  $\sigma$ . Depending on  $\lambda$ , it can behave in three different ways: In the absence of regularization,  $J_2^a$  becomes arbitrarily large for  $\sigma$  small or large enough and enjoys a global minimum,  $\sigma_0$ , which is consistent with the left panel of Figure 1. However, as soon as regularization is added,  $J_2^a$  goes to 0 as bandwidth goes to infinity, as indicated in the right panel. As long as the regularization parameter  $\lambda \leq 2ne^{-3/2} \approx 0.45n$ , there still exists a local minimum at  $\sigma_0$ . This is further illustrated in Figure 2, where we plot  $J_2^a$  together with its components  $j_a$  and  $j_b$  for three different values of  $\lambda$ , reflecting the three types of behavior. Since  $j_b$  is bounded by  $1/\lambda$ , for  $\lambda$  large enough it is negligible compared to  $j_a$ .

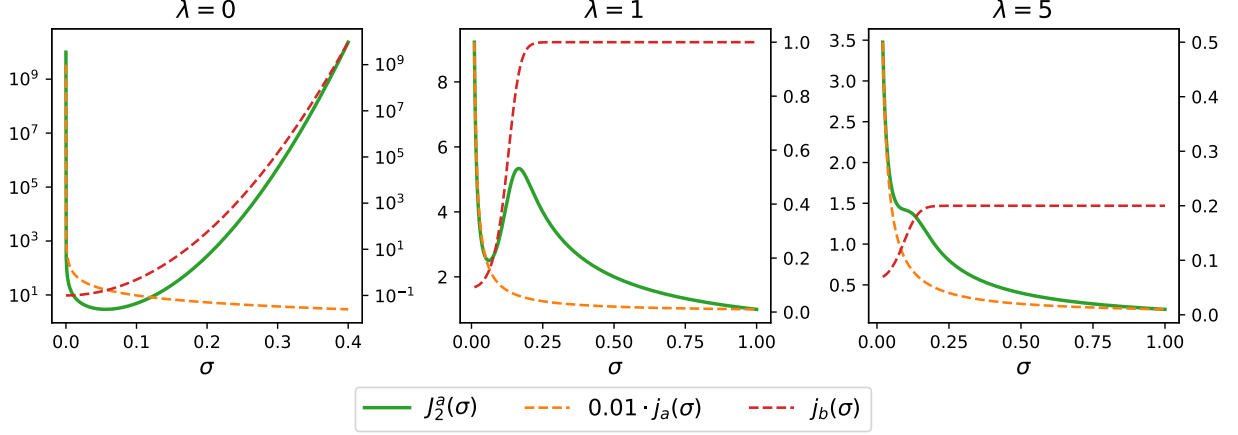


Figure 2: Approximate Jacobian norm,  $J_2^a$ , (left y-axis), and its two factors,  $j_a$  and  $j_b$ , (right y-axis), as defined in Equations 4 and 5, as functions of the bandwidth for three different values of  $\lambda$ , and  $n = 10$ ,  $l_{\max} = 1$ ,  $p = 1$ . Note that the scales of the axes differ between the three panels and that  $j_a(\sigma)$  is scaled down by a factor of 100. We clearly see the global and local minima stated in Proposition 1. For  $\lambda = 0$ ,  $J_2^a(0) = J_2^a(\infty) = +\infty$  with a global minimum at  $\sigma_0$ . For  $\lambda > 0$ ,  $J_2^a(0) = +\infty$  and  $J_2^a(\infty) = 0$ . For  $\lambda \leq 2ne^{-3/2}$ ,  $J_2^a$  has a local minimum at  $\sigma_0$ .  $j_a(\sigma)$  decreases monotonically to 0, while  $j_b(\sigma)$  increases monotonically to  $1/\lambda$ .

**Proposition 1.**

Let  $J_2^a(\sigma)$  be defined according to Definition 1, and let, for  $k \in \{-1, 0\}$ ,

$$\sigma_k := \frac{\sqrt{2}}{\pi} \frac{l_{\max}}{(n-1)^{1/p} - 1} \sqrt{1 - 2W_k\left(-\frac{\lambda\sqrt{e}}{2n}\right)}, \quad (6)$$

where  $W_k$  denotes the  $k$ -th branch of the Lambert  $W$  function. Then

- For  $\lambda = 0$ ,  $J_2^a(0) = J_2^a(\infty) = +\infty$ , and  $J_2^a(\sigma_0) = J_2^a\left(\frac{\sqrt{2}}{\pi} \frac{l_{\max}}{(n-1)^{1/p} - 1}\right)$  is a global minimum.
- For  $0 < \lambda \leq 2ne^{-3/2}$ ,  $J_2^a(0) = +\infty$ , and  $J_2^a(\infty) = 0$ , with a local minimum  $J_2^a(\sigma_0)$  and a local maximum  $J_2^a(\sigma_{-1})$ .
- For  $\lambda > 2ne^{-3/2}$ , neither  $\sigma_0$  nor  $\sigma_{-1}$  is defined and  $J_2^a(\sigma)$  decreases monotonically from  $J_2^a(0) = +\infty$  to  $J_2^a(\infty) = 0$ .

*Sketch of Proof.* We evaluate  $J_2^a(0)$ ,  $J_2^a(\infty)$  and points where  $\frac{\partial J_2^a(\sigma)}{\partial \sigma} = 0$  to obtain extreme point candidates. To avoid infeasible solutions, we have to consider the domain of the Lambert  $W$  function. For the full proof, see Appendix A.  $\square$

Based on Proposition 1 we can now propose a bandwidth selection scheme based on Jacobian control: For  $\lambda \leq 2ne^{-3/2}$ , we choose the (possibly local) minimum  $\sigma_0$  as our Jacobian based bandwidth. For  $\lambda > 2ne^{-3/2}$ ,  $\sigma_0$  is not defined; in this case we choose our bandwidth as if  $\lambda = 2ne^{-3/2}$ . Note that  $\sigma_0$  is quite stable to changes in  $\lambda$ : The square root expression in Equation 6 increases from 1 for  $\lambda = 0$  to  $\sqrt{3}$  for  $\lambda = 2ne^{-3/2}$ . This stability in terms of  $\lambda$  can be seen in Figures 2 and 3.

## 2.1 Theoretical Details

In this section, we present the calculations behind Definition 1. We also illuminate how bandwidth selection is a trade-off between a well-conditioned training data kernel matrix and a slow decay of the inferred function toward the default value.

We first use Proposition 2 to approximate the norm of the two kernel matrices in Equation 2 with a product of two matrix norms. We then use Propositions 3 and 4 to estimate these two norms for the case of the Gaussian kernel. Note that Proposition 2 holds for any kernel, not only the Gaussian.

**Proposition 2.**

Let  $\mathbf{d}_i := \mathbf{x}^* - \mathbf{x}_i$  where  $\mathbf{x}_i$  is a row in  $\mathbf{X}$ . Then, with  $\hat{f}(\mathbf{x}^*)$  according to Equation 2, for any function  $k(\mathbf{x}, \mathbf{x}')$ ,

$$\begin{aligned} \left\| \frac{\partial \hat{f}(\mathbf{x}^*)}{\partial \mathbf{x}^*} \right\|_2 &= \left\| \frac{\partial \hat{f}(\mathbf{x}^*)}{\partial \mathbf{d}_i} \right\|_2 \\ &\leq \max_{\mathbf{x}_i \in \mathbf{X}} \left\| \frac{\partial k(\mathbf{x}^*, \mathbf{x}_i)}{\partial \mathbf{x}^*} \right\|_1 \cdot \left\| (\mathbf{K}(\mathbf{X}, \mathbf{X}) + \lambda \mathbf{I})^{-1} \right\|_2 \cdot \sqrt{n} \|\mathbf{y}\|_2 \\ &= \max_{\mathbf{x}_i \in \mathbf{X}} \left\| \frac{\partial k(\mathbf{d}_i + \mathbf{x}_i, \mathbf{x}_i)}{\partial \mathbf{d}_i} \right\|_1 \cdot \left\| (\mathbf{K}(\mathbf{X}, \mathbf{X}) + \lambda \mathbf{I})^{-1} \right\|_2 \cdot \sqrt{n} \|\mathbf{y}\|_2, \end{aligned} \quad (7)$$

where the matrix norms are the induced operator norms.

*Sketch of Proof.* We first use submultiplicativity to split the norm into three factors, and equivalence of matrix norms to replace the 2-norm with the 1-norm in the first factor. Finally, we show that  $\frac{\partial \hat{f}(\mathbf{x}^*)}{\partial \mathbf{x}^*} = \frac{\partial \hat{f}(\mathbf{x}^*)}{\partial \mathbf{d}_i}$  to obtain the forms for the two factors. For the full proof, see Appendix A.  $\square$

**Proposition 3.**

Let  $\mathbf{d}_i := \mathbf{x}^* - \mathbf{x}_i$  where  $\mathbf{x}_i$  is a row in  $\mathbf{X}$ , and denote  $d_i := \|\mathbf{d}_i\|_2$ . Then, for the Gaussian kernel,

$$k_G(\mathbf{d}_i, \sigma) = \exp\left(-\frac{\|\mathbf{d}_i\|_2^2}{2\sigma^2}\right),$$

$$\max_{\mathbf{x}_i \in \mathbf{X}} \left\| \frac{\partial k_G(\mathbf{d}_i, \sigma)}{\partial \mathbf{d}_i} \right\|_1 = \max_{\mathbf{x}_i \in \mathbf{X}} \frac{d_i}{\sigma^2} \exp\left(-\frac{d_i^2}{2\sigma^2}\right) \leq \frac{1}{\sigma\sqrt{e}} =: \frac{1}{\sqrt{e}} \cdot j_a(\sigma). \quad (8)$$

*Sketch of Proof.* Since the Gaussian kernel is rotationally invariant we only need to consider the radial coordinate,  $d_i$ , when calculating the gradient. The value of  $d_i$  that maximizes the gradient is calculated by setting the derivative (of the gradient) to zero. For the full proof, see Appendix A.  $\square$

**Proposition 4.**

For  $\mathbf{K}(\mathbf{X}, \mathbf{X}, \sigma)_{ij} = k_G(\mathbf{x}_i, \mathbf{x}_j, \sigma)$ , where  $k_G(\mathbf{x}, \mathbf{x}', \sigma)$  denotes the Gaussian kernel,

$$\left\| (\mathbf{K}(\mathbf{X}, \mathbf{X}, \sigma) + \lambda \mathbf{I})^{-1} \right\|_2 \geq \frac{1}{n \cdot \exp\left(-\left(\frac{((n-1)^{1/p}-1)\pi\sigma}{2l_{\max}}\right)^2\right) + \lambda} =: j_b(\sigma). \quad (9)$$

*Sketch of Proof.* Bermanis et al. (2013) provide an estimate for the number of singular values larger than  $\delta \cdot s_1$  for a Gaussian kernel matrix, where  $\delta > 0$  and  $s_1$  denotes the largest singular value. Using this expression, we can upper bound the smallest singular value, or, equivalently, lower bound the largest singular value of the inverse matrix. The addition of  $\lambda \mathbf{I}$  shifts all singular values by  $\lambda$ . For the full proof, see Appendix A.  $\square$

In the absence of regularization,  $j_b(\sigma)$  is a bound of the spectral norm of the inverse training data kernel matrix. With increasing  $\sigma$ , the elements in  $\mathbf{K}(\mathbf{X}, \mathbf{X}, \sigma)$  become increasingly similar, and  $\mathbf{K}(\mathbf{X}, \mathbf{X}, \sigma)$  becomes closer to singular, which results in an ill-conditioned solution, where  $\hat{f}(\mathbf{x}^*)$  is very sensitive to perturbations in  $\mathbf{X}$ . Introducing regularization controls the conditioning, as seen in Figure 2;  $j_b(\sigma)$  is upper bounded by  $1/\lambda$ . The poor generalization properties of regression with an ill-conditioned kernel matrix are well known, see e.g. Poggio et al. (2019), Amini (2021), or Hastie et al. (2022).

With the Jacobian approach, the contribution of an ill-conditioned matrix,  $j_b(\sigma)$ , is balanced by how quickly the inferred function decays in the absence of training data,  $j_a(\sigma)$ . For a too small bandwidth, the inferred function quickly decays to zero;  $j_a(\sigma)$  is large and thus the derivatives of the inferred function. For a too large bandwidth,  $\mathbf{K}(\mathbf{X}, \mathbf{X}, \sigma)$  is almost singular, which results in extreme predictions;  $j_b(\sigma)$  is large, and thus the derivatives of the inferred function. By controlling the Jacobian, both poor generalization due to predicting mostly zero and poor generalization due to extreme predictions is avoided.

Table 1: Real data sets used for comparing the four bandwidth selection methods.

Data Set	Size, $n \times p$
Quality of aspen tree fibres <sup>1</sup>	$25165 \times 5$
Appliances energy use in a low energy building in Stambruges, Belgium (Candanedo et al., 2017) <sup>2</sup>	$19735 \times 27$
House values in California (Pace and Barry, 1997) <sup>3</sup>	$20640 \times 8$
Protein structure as root-mean-square deviation of atomic positions, taken from CASP <sup>4</sup>	$45730 \times 9$
Daily concentration of black smoke particles in the U.K. in the year 2000 (Wood et al., 2017) <sup>5</sup>	$45568 \times 10$

## 2.2 Outlier Sensitivity

Since  $l_{\max}$  might be sensitive to outliers, Equation 6 suggests that so might the Jacobian method. One option to mitigate this problem is to use a trimmed version of  $l_{\max}$ , calculated after removing outliers. Our approach is however based on the observation that for data evenly spread within a hypercube in  $\mathbb{R}^p$  with side  $l_{\max}$ ,  $\frac{l_{\max}}{(n-1)^{1/p}-1}$  is exactly the distance from an observation to its closest neighbor(s). We thus define the Jacobian median method analogously to the Jacobian method but with  $\frac{l_{\max}}{(n-1)^{1/p}-1}$  replaced by  $\text{Med}_{i=1}^n (\min_{j \neq i} \|\mathbf{x}_i - \mathbf{x}_j\|_2)$ , i.e. median of the closest-neighbor-distances.

## 3 Experiments

Experiments were performed on one synthetic and seven real data sets. The metrics evaluated were test  $R^2$ , i.e. the proportion of the variation in the data that is explained by the model, the selected bandwidth  $\sigma$ , and bandwidth selection computation time in milliseconds,  $t$ . In all experiments, the Jacobian-based bandwidth was compared to those of generalized cross-validation (GCV) for kernel regression (Hastie et al., 2022), marginal likelihood maximization (MML), and Silverman’s rule of thumb. Note, however, that Silverman’s method was developed with KDE, rather than KRR, in mind and thus does not take  $\lambda$  into account. We chose however to include it as a reference since, just like the Jacobian method, it is a computationally light, closed-form solution. To avoid singular matrices, a small regularization of  $\lambda = 10^{-3}$  was used in all experiments unless otherwise stated. All experiments were run on a cluster with Intel Xeon Gold 6130 CPUs.

In Section 3.1, we perform experiments on five large data sets, focusing on performance, in terms of  $R^2$  and computation time, while in Section 3.2, we perform experiments on relatively simple data sets, to demonstrate the similarities and differences between the four bandwidth selection methods in greater detail.

### 3.1 Large Real Data

In this section, we compare the bandwidth selection methods on the five real data sets described in Table 1. The data sets were selected to compare the algorithms on a diverse set of applications, although they all have in common that they are relatively large in terms of number of observations and dimensions.

For each data set, 100 random splits were created by selecting 10000 of the observations at random. For each split, the data was standardized and split randomly into 65 % training and 45 % testing data. For cross-validation, 10 logarithmically spaced values between 0.001 and  $l_{\max}$  were used.

In Table 2, we present the means together with the first and ninth deciles for  $R^2$ , and  $t$  across the 100 splits for each method, together with the results of Wilcoxon signed rank tests, testing whether the Jacobian method performs better (in terms of explained variance) and faster (in terms of computation time) than the competing methods. On the evaluated data, the Jacobian method is up to a million times faster than GCV and MML, while generally performing on par, or better, in terms of  $R^2$ . Compared to MML, the Jacobian method performs significantly better on four of the five data

<sup>1</sup>The data set is available at <https://openmv.net/info/wood-fibres>.

<sup>2</sup>The data set is available at <https://github.com/LuisM78/Appliances-energy-prediction-data>.

<sup>3</sup>The data set is available at [https://www.dcc.fc.up.pt/~ltorgo/Regression/cal\\_housing.html](https://www.dcc.fc.up.pt/~ltorgo/Regression/cal_housing.html).

<sup>4</sup><https://predictioncenter.org/>, the data set is available at <https://archive.ics.uci.edu/ml/datasets/Physicochemical+Properties+of+Protein+Tertiary+Structure>.

<sup>5</sup>The data set is available at <https://www.maths.ed.ac.uk/~swood34>.

Table 2: Mean together with first and ninth deciles (within parentheses) of explained variance,  $R^2$ , and bandwidth selection time in seconds,  $t$ , for the five data sets from Table 1. In the second rows of the cells, we state the p-values of Wilcoxon signed rank tests, testing whether the Jacobian method performs better (in terms of explained variance) and/or faster (in terms of computation time) than the competing method. In all cases, the Jacobian method is significantly faster than the competing methods, and, in most cases, it performs significantly better.

Aspen Fibres	Jacobian	0.65 (0.62, 0.67)	0.00031 (0.00016, 0.00043)
	GCV	0.65 (0.63, 0.67) $p_{\text{Wil}} = 0.59$	520 (350, 690) $p_{\text{Wil}} = \mathbf{1.9 \cdot 10^{-18}}$
	MML	0.61 (0.59, 0.64) $p_{\text{Wil}} = \mathbf{1 \cdot 10^{-17}}$	280 (240, 330) $p_{\text{Wil}} = \mathbf{1.9 \cdot 10^{-18}}$
	Silverman	0.49 (0.45, 0.53) $p_{\text{Wil}} = \mathbf{1.9 \cdot 10^{-18}}$	0.00045 (0.00029, 0.00073) $p_{\text{Wil}} = \mathbf{5.5 \cdot 10^{-16}}$
Appliances Energy Use	Jacobian	0.26 (0.24, 0.28)	0.00036 (0.00026, 0.00042)
	GCV	0.27 (0.24, 0.3) $p_{\text{Wil}} = 1$	200 (180, 220) $p_{\text{Wil}} = \mathbf{1.9 \cdot 10^{-18}}$
	MML	0.27 (0.24, 0.29) $p_{\text{Wil}} = 1$	240 (210, 270) $p_{\text{Wil}} = \mathbf{1.9 \cdot 10^{-18}}$
	Silverman	0.18 (0.16, 0.21) $p_{\text{Wil}} = \mathbf{1.9 \cdot 10^{-18}}$	0.0011 (0.00086, 0.0017) $p_{\text{Wil}} = \mathbf{2.9 \cdot 10^{-17}}$
California Housing	Jacobian	0.59 (0.29, 0.71)	0.00034 (0.00017, 0.00044)
	GCV	0.7 (0.59, 0.75) $p_{\text{Wil}} = 1$	590 (340, 790) $p_{\text{Wil}} = \mathbf{1.9 \cdot 10^{-18}}$
	MML	0.38 (-0.045, 0.65) $p_{\text{Wil}} = \mathbf{8.8 \cdot 10^{-8}}$	260 (240, 280) $p_{\text{Wil}} = \mathbf{1.9 \cdot 10^{-18}}$
	Silverman	0.5 (0.45, 0.55) $p_{\text{Wil}} = \mathbf{2.9 \cdot 10^{-7}}$	0.00054 (0.00039, 0.00083) $p_{\text{Wil}} = \mathbf{1.9 \cdot 10^{-18}}$
Protein Structure	Jacobian	0.37 (0.35, 0.39)	0.00033 (0.00018, 0.00042)
	GCV	0.42 (0.39, 0.44) $p_{\text{Wil}} = 1$	460 (400, 510) $p_{\text{Wil}} = \mathbf{1.9 \cdot 10^{-18}}$
	MML	0.32 (0.3, 0.33) $p_{\text{Wil}} = \mathbf{1.9 \cdot 10^{-18}}$	300 (240, 370) $p_{\text{Wil}} = \mathbf{1.9 \cdot 10^{-18}}$
	Silverman	0.14 (0.086, 0.19) $p_{\text{Wil}} = \mathbf{1.9 \cdot 10^{-18}}$	0.00066 (0.00043, 0.0011) $p_{\text{Wil}} = \mathbf{1.9 \cdot 10^{-18}}$
U.K. Black Smoke	Jacobian	0.31 (0.29, 0.33)	0.00032 (0.00016, 0.00041)
	GCV	0.31 (0.3, 0.33) $p_{\text{Wil}} = 1$	380 (330, 420) $p_{\text{Wil}} = \mathbf{1.9 \cdot 10^{-18}}$
	MML	0.27 (0.26, 0.29) $p_{\text{Wil}} = \mathbf{1.9 \cdot 10^{-18}}$	240 (220, 270) $p_{\text{Wil}} = \mathbf{1.9 \cdot 10^{-18}}$
	Silverman	0.16 (0.12, 0.19) $p_{\text{Wil}} = \mathbf{1.9 \cdot 10^{-18}}$	0.00056 (0.00041, 0.0011) $p_{\text{Wil}} = \mathbf{2.7 \cdot 10^{-17}}$

sets, while GCV tends to perform slightly better than the Jacobian method. Silverman’s method also performs well in terms of computation time but performs significantly worse than the Jacobian method in terms of  $R^2$ .

### 3.2 Synthetic and Simpler Real Data

In this section, we compare the four methods on the following data:

- 2D Temperature Data: The temperatures at 40 different French weather stations at 3 a.m., Jan 1st, 2020.
- 1D Temperature Data: The temperature at 248 different times in January 2020 at the weather station at Toulouse-Blagnac.
- Cauchy Synthetic Data: For  $n$  observations, for  $i \in [1, n]$ ,  $x_i \sim \text{Cauchy}(0, 3)$ ,  $y_i = \sin(2\pi x_i) + \varepsilon_i$ , where  $\varepsilon_i \sim \mathcal{N}(0, 0.2^2)$ .

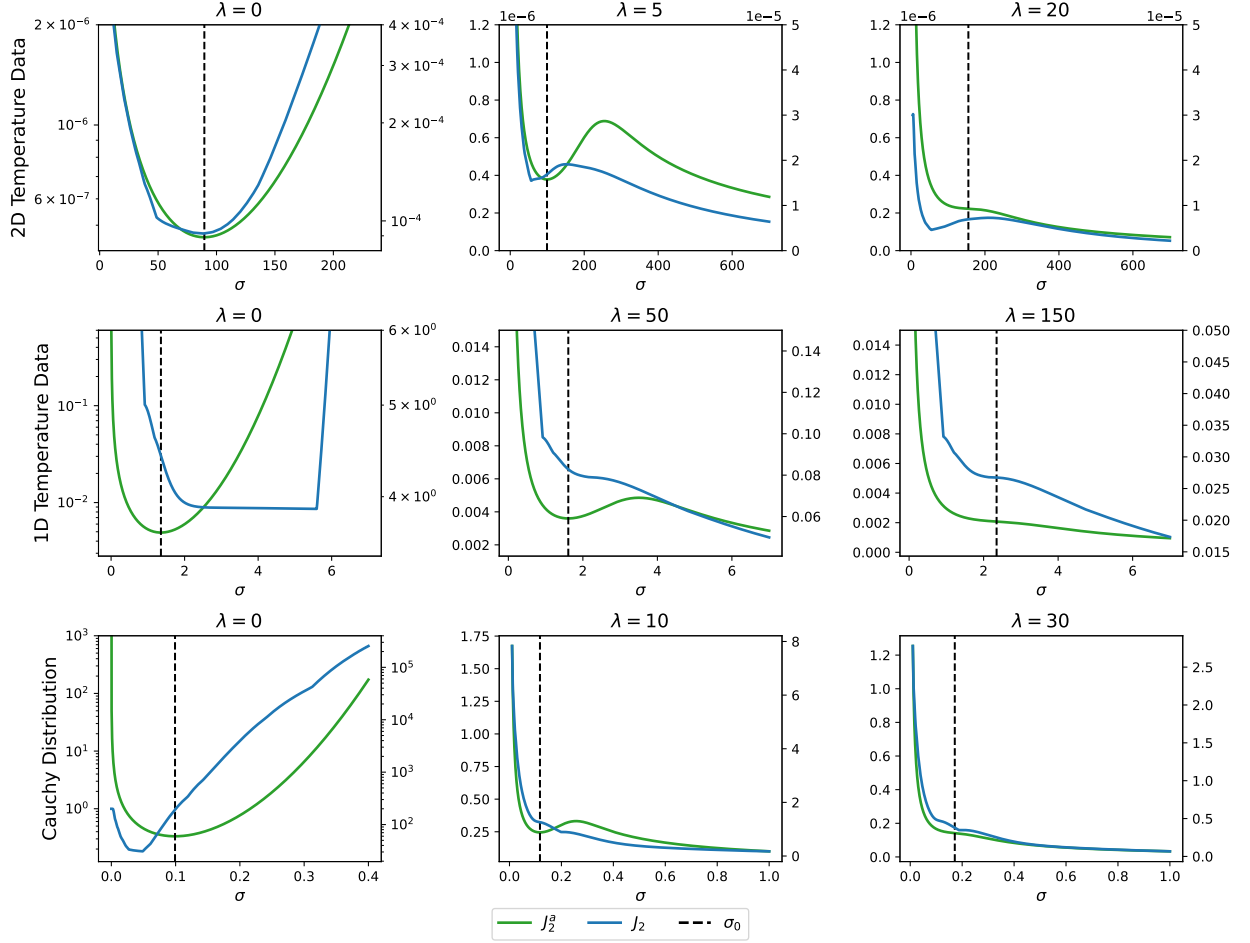


Figure 3: Comparison of the approximate (green, left y-axis) and true (blue, right y-axis) Jacobian norms as a function of bandwidth and regularization. The approximate Jacobian norm captures the structure of the true Jacobian norm quite well, especially for the 2D temperature data, where for  $\lambda = 0$ , the minima of the two functions agree very well. For  $\lambda > 0$ , the selected bandwidth,  $\sigma_0$ , is close to the elbow of both the approximate and true norms. In the rightmost panel,  $\lambda > 2ne^{-3/2}$ , which means that the approximate Jacobian norm has no local minimum and  $\sigma_0$  is selected as if  $\lambda = 2ne^{-3/2}$ .

The French temperature data was obtained from Météo France<sup>6</sup> and processed following the setup by Vanwysberghe (2021). For the cross-validation, 100 logarithmically spaced values between 0.001 and  $l_{\max}$  were used.

In Figure 3, we compare the approximate and true Jacobian norms as functions of the bandwidth. We see that the approximate norm captures the structure of the true norm quite well. In the absence of regularization, the minima of the two functions approximately agree. When regularization is added, the selected bandwidth,  $\sigma_0$ , is close to the elbow of both the approximate and true norms.

In Figures 4 and 5, we provide the results of jackknife resampling for the two temperature data sets. For each data set, the experiments were repeated  $n$  times, omitting a different observation in each experiment. For the 1D temperature data, half of the observations were set aside as reference data. Apart from plotting the jackknife mean and standard deviations of the prediction, we also state the mean and standard deviations of the selected bandwidths. Compared to the other methods, the Jacobian method tends to provide less extreme predictions and to be more stable in terms of selected bandwidth across the experiments. For the 1D data, the predictions provided by MML and Silverman's method are admittedly the least extreme, but at the expense of failing to capture the dynamics of the data.

<sup>6</sup>The data set is available at [https://donneespubliques.meteofrance.fr/donnees\\_libres/Txt/Synop/postesSynop.csv](https://donneespubliques.meteofrance.fr/donnees_libres/Txt/Synop/postesSynop.csv)

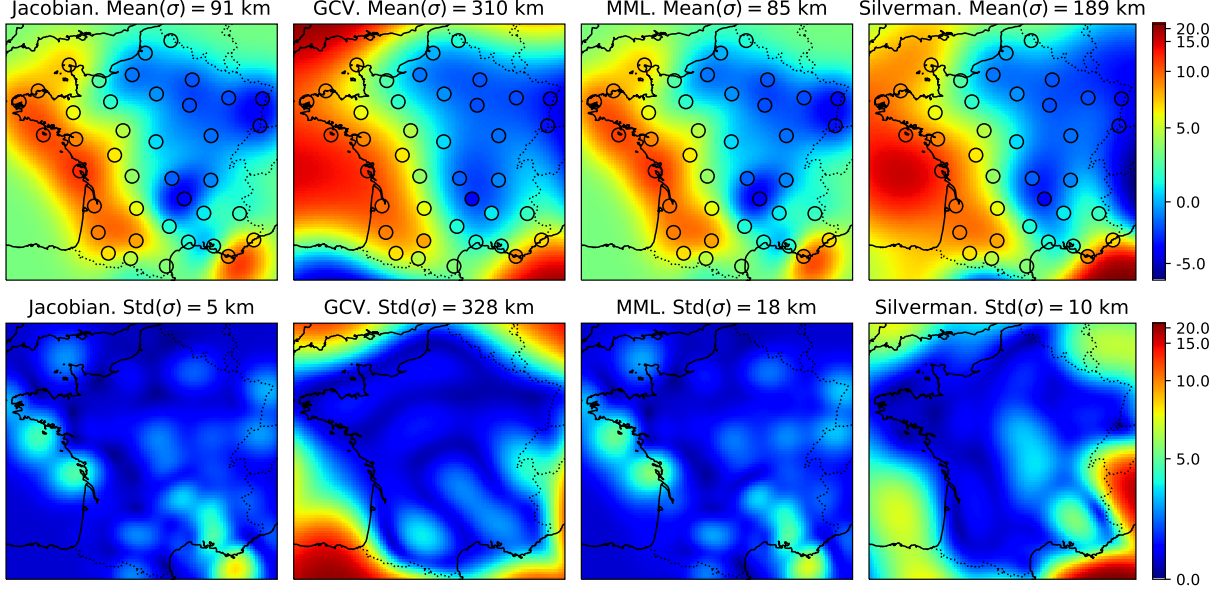


Figure 4: Means (top row) and standard deviations (bottom row) of KRR temperature predictions in  $^{\circ}\text{C}$  from jackknife resampling on the 2D temperature data. Note that the scales are not linear. The Jacobian and MML methods provide less extreme predictions than GCV and Silverman’s method does. They are also more stable in terms of bandwidth selection.

### 3.2.1 Varying Sample Size and Regularization

In Figures 6 and 7, we vary the sample size,  $n$ , and regularization strength,  $\lambda$ . For the synthetic data, 1000 test observations were generated, while the real data was randomly split into training and testing data. When varying  $n$ , 15 % of the real data was saved for testing, resulting in splits of size  $n/6$ ,  $n/37$ , and  $n/1000$  for the 2D temperature, 1D temperature, and synthetic data, respectively. When varying  $\lambda$ ,  $n$  was chosen to a value where the different methods performed approximately equally well in the experiments with varying sample size (Figure 6). Thus the splits when varying  $\lambda$  were 25/15, 100/148, and 50/1000 for the 2D temperature, 1D temperature, and synthetic data, respectively. In all cases 1000 random splits were used to estimate the variance of test  $R^2$ , the selected bandwidth  $\sigma$ , and the bandwidth selection computation time,  $t$ . It is again confirmed that the Jacobian method, in addition to being much faster than GCV and MML, is much more stable in terms of bandwidth selection. For the Cauchy distributed data, the median version of the Jacobian method was used; this method requires slightly more time than the standard Jacobian method. The reason for Silverman’s method being slower than the Jacobian method for the 2D temperature data is due to its need to calculate the standard deviation of the data, and thus the distance to the mean from all observations. For the 2D temperature data, calculating the distances comprises a larger fraction of the calculations than for the other data. The other three methods do not use the standard deviation and are thus less affected.

## 4 Conclusions

We proposed a computationally low-cost method for choosing the bandwidth for kernel ridge regression with the Gaussian kernel. The method was motivated by the observed improved generalization properties of neural networks trained with Jacobian regularization. By selecting a bandwidth with Jacobian control, we implicitly constrain the derivatives of the inferred function. To achieve this, we derived a simple, closed-form approximate expression for the Jacobian of Gaussian KRR as a function of the bandwidth and were thus able to find an optimal bandwidth for Jacobian control. We demonstrated how selecting the optimal bandwidth is a trade-off between utilizing a well-conditioned training data kernel matrix and a slow decay of the inferred function toward the default value.

In terms of model performance, our method is on par with cross-validation and marginal likelihood maximization, but up to a million times faster on the considered data. Compared to Silverman’s method, our method is superior in terms of model performance.

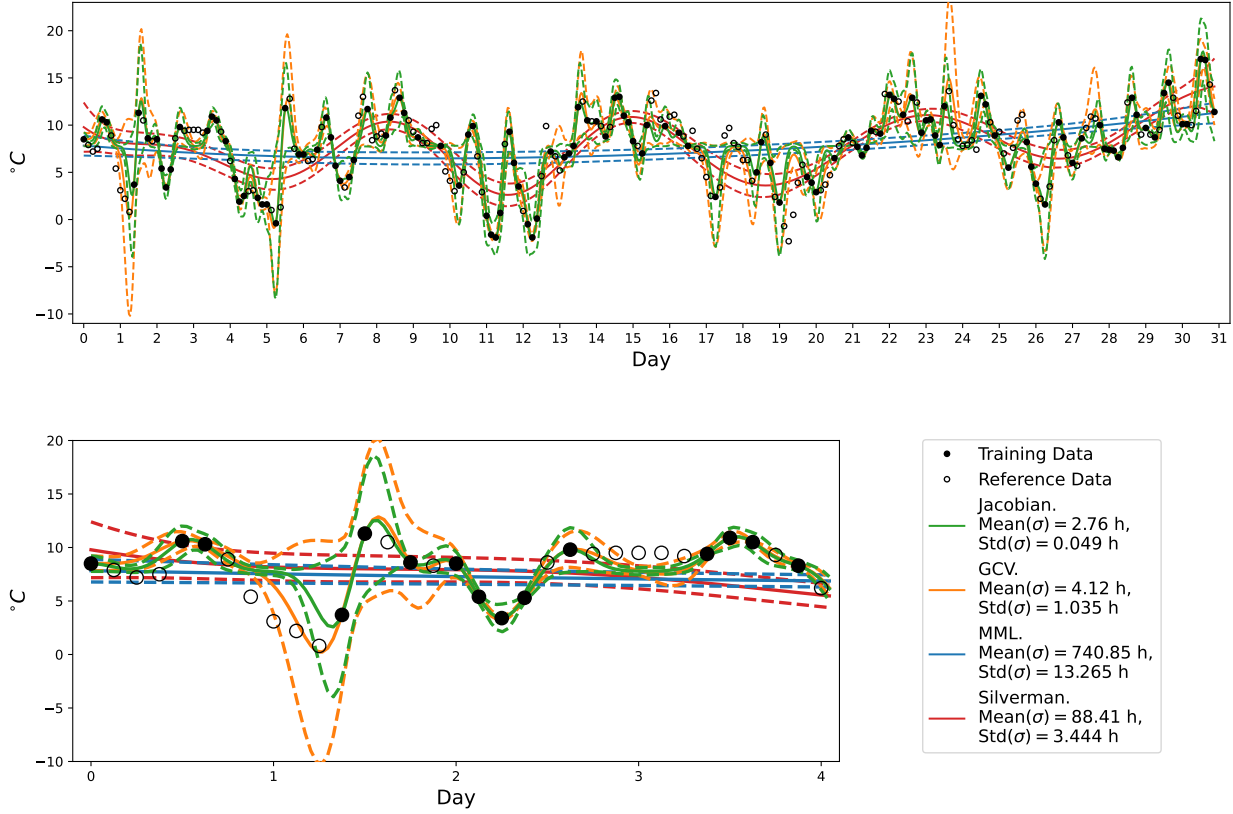


Figure 5: Means and standard deviations of KRR predictions from jackknife resampling on the 1D temperature data. The lower bottom plot shows a zoom-in on the first 4 days. The Jacobian method performs similarly to cross-validation but provides slightly less extreme predictions. It is also more stable in terms of bandwidth selection. MML and Silverman’s methods both underfit the data, which can be attributed to their much larger bandwidth.

Even though we only considered Jacobian bandwidth selection for the Gaussian kernel, the principle holds for any kernel. That, however, requires new, kernel-specific, estimates of the kernel matrix norms. Similarly, in the Gaussian case, the estimate of the norm of the inverse kernel matrix could potentially be further improved. These research problems are left for future work.

Code is available at [https://github.com/allerbo/jacobian\\_bandwidth\\_selection](https://github.com/allerbo/jacobian_bandwidth_selection).

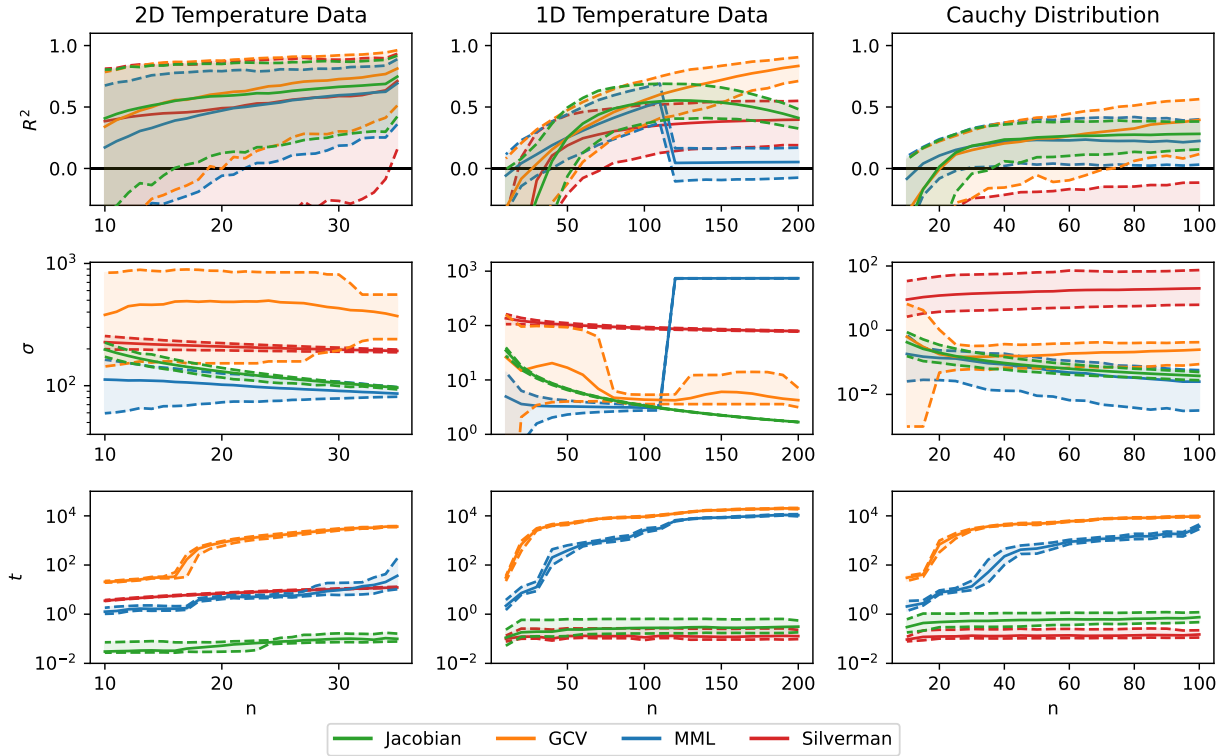


Figure 6: Mean together with first and ninth deciles for explained variance on test data,  $R^2$ ; selected bandwidth,  $\sigma$ ; and computation time in milliseconds  $t$ , for different training sample sizes, using the four bandwidth selection methods. The Jacobian and Silverman's methods are several orders of magnitude faster than the two other methods. They are also much more stable in terms of bandwidth selection. In terms of prediction, the Jacobian method generally performs better than, or on par with, the competing methods, except compared to cross-validation when  $n$  is large. For the 1D temperature data, MML gets stuck in a local minimum. For the Cauchy data, the, slightly slower, median version of the Jacobian method was used.

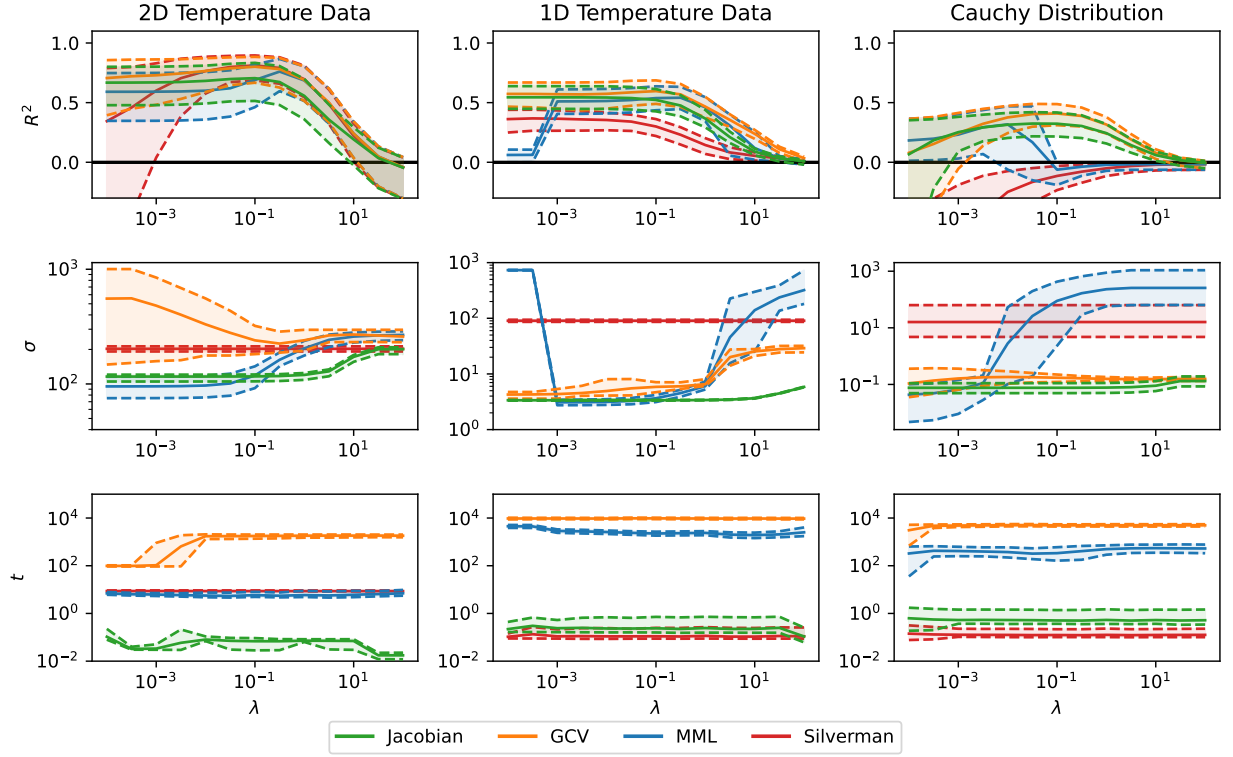


Figure 7: Mean together with first and ninth deciles for explained variance on test data,  $R^2$ ; selected bandwidth,  $\sigma$ ; and computation time in milliseconds  $t$ , for different regularization strengths, using the four bandwidth selection methods. The Jacobian and Silverman's methods are several orders of magnitude faster than the two other methods. They are also much more stable in terms of bandwidth selection. In terms of prediction, the Jacobian method generally performs better than, or on par with, the competing methods. For both the 1D temperature data and the Cauchy data, MML gets stuck in local minima. For the Cauchy data, the, slightly slower, median version of the Jacobian method was used.

## A Proofs

*Proof of Proposition 1.*

Denote  $d := \frac{2l_{\max}}{((n-1)^{1/p}-1)\pi}$ . Then

$$J_2^a(\sigma, l, n, p, \lambda) = J_2^a(\sigma, n, d, \lambda) = \frac{1}{\sigma \left( n \exp \left( - \left( \frac{\sigma}{d} \right)^2 \right) + \lambda \right)},$$

from which we obtain

$$\lim_{\sigma \rightarrow 0^+} J_2^a(\sigma) = +\infty$$

and

$$\lim_{\sigma \rightarrow +\infty} J_2^a(\sigma) = \begin{cases} +\infty & \text{if } \lambda = 0 \\ 0 & \text{if } \lambda > 0. \end{cases}$$

We now identify stationary points by setting the derivative to 0.

$$\begin{aligned} \frac{\partial J_2^a(\sigma)}{\partial \sigma} &= - \frac{\exp \left( \left( \frac{\sigma}{d} \right)^2 \right) \left( n + \lambda \exp \left( \left( \frac{\sigma}{d} \right)^2 \right) - 2n \left( \frac{\sigma}{d} \right)^2 \right)}{\left( \sigma \left( n + \lambda \exp \left( \left( \frac{\sigma}{d} \right)^2 \right) \right) \right)^2}. \\ n + \lambda e^{\left( \frac{\sigma}{d} \right)^2} - 2n \left( \frac{\sigma}{d} \right)^2 &= 0 \iff -\frac{\lambda \sqrt{e}}{2n} = e^{\frac{1}{2} - \left( \frac{\sigma}{d} \right)^2} \left( \frac{1}{2} - \left( \frac{\sigma}{d} \right)^2 \right) \\ \iff \left( \frac{1}{2} - \left( \frac{\sigma}{d} \right)^2 \right) &= W \left( -\frac{\lambda \sqrt{e}}{2n} \right) \implies \sigma = \frac{d}{\sqrt{2}} \sqrt{1 - 2W \left( -\frac{\lambda \sqrt{e}}{2n} \right)}, \end{aligned}$$

where  $W$  denotes the Lambert  $W$  function. Since this function has real outputs only if its argument is greater than  $-e^{-1}$ , in order to obtain stationary points we need

$$-\frac{\lambda \sqrt{e}}{2n} \geq -e^{-1} \iff \lambda \leq 2ne^{-3/2}$$

which gives us the two stationary points

$$\sigma_0 = \frac{\sqrt{2}}{\pi} \frac{l_{\max}}{(n-1)^{1/p}-1} \sqrt{1 - 2W_0 \left( -\frac{\lambda \sqrt{e}}{2n} \right)}$$

and

$$\sigma_{-1} = \frac{\sqrt{2}}{\pi} \frac{l_{\max}}{(n-1)^{1/p}-1} \sqrt{1 - 2W_{-1} \left( -\frac{\lambda \sqrt{e}}{2n} \right)}.$$

$W_{-1}(x) < W_0(x)$  for  $x \in (-e^{-1}, 0)$ , which implies that  $\sigma_0 < \sigma_{-1}$ . Combined with the limits above, this implies that, when existing,  $\sigma_0$  is a local minimum and  $\sigma_{-1}$  is a local maximum.

Finally, for  $\lambda = 0$ ,  $W_0(0) = 0$  and  $\lim_{\lambda \rightarrow 0} W_{-1} \left( -\frac{\lambda \sqrt{e}}{2n} \right) = -\infty$ , which means that in the absence of  $\lambda$ ,  $\sigma_0 = \frac{\sqrt{2}}{\pi} \frac{l_{\max}}{(n-1)^{1/p}-1}$  and  $\sigma_{-1} = +\infty$ .  $\square$

*Proof of Proposition 2.*

We first note that for  $\mathbf{d}_i = \mathbf{x}^* - \mathbf{x}_i$ ,  $\frac{\partial \hat{f}(\mathbf{x}^*)}{\partial \mathbf{d}_i} = \frac{\partial \hat{f}(\mathbf{x}^*)}{\partial \mathbf{x}^*}$ :

$$\begin{aligned} \frac{\partial \mathbf{d}_i}{\partial \mathbf{x}^*} &= \frac{\partial (\mathbf{x}^* - \mathbf{x}_i)}{\partial \mathbf{x}^*} = \frac{\partial \mathbf{x}^*}{\partial \mathbf{x}^*} - \frac{\partial \mathbf{x}_i}{\partial \mathbf{x}^*} = \mathbf{I} - \mathbf{0} = \mathbf{I} \\ \frac{\partial \hat{f}(\mathbf{x}^*)}{\partial \mathbf{x}^*} &= \frac{\partial \hat{f}(\mathbf{x}^*)}{\partial \mathbf{d}_i} \cdot \frac{\partial \mathbf{d}_i}{\partial \mathbf{x}^*} = \frac{\partial \hat{f}(\mathbf{x}^*)}{\partial \mathbf{d}_i} \cdot \mathbf{I} = \frac{\partial \hat{f}(\mathbf{x}^*)}{\partial \mathbf{d}_i}. \end{aligned}$$

Now,

$$\begin{aligned}
\left\| \frac{\partial \hat{f}(\mathbf{x}^*)}{\partial \mathbf{d}_i} \right\|_2 &= \left\| \frac{\partial \hat{f}(\mathbf{x}^*)}{\partial \mathbf{x}^*} \right\|_2 = \left\| \frac{\partial}{\partial \mathbf{x}^*} \left( \mathbf{k}(\mathbf{x}^*, \mathbf{X})^\top \cdot (\mathbf{K}(\mathbf{X}, \mathbf{X}) + \lambda \mathbf{I})^{-1} \cdot \mathbf{y} \right) \right\|_2 \\
&= \left\| \frac{\partial \mathbf{k}(\mathbf{x}^*, \mathbf{X})^\top}{\partial \mathbf{x}^*} \cdot (\mathbf{K}(\mathbf{X}, \mathbf{X}) + \lambda \mathbf{I})^{-1} \mathbf{y} \right\|_2 \\
&\leq \left\| \frac{\partial \mathbf{k}(\mathbf{x}^*, \mathbf{X})^\top}{\partial \mathbf{x}^*} \right\|_2 \cdot \left\| (\mathbf{K}(\mathbf{X}, \mathbf{X}) + \lambda \mathbf{I})^{-1} \right\|_2 \cdot \|\mathbf{y}\|_2 \\
&\leq \sqrt{n} \cdot \left\| \frac{\partial \mathbf{k}(\mathbf{x}^*, \mathbf{X})^\top}{\partial \mathbf{x}^*} \right\|_1 \cdot \left\| (\mathbf{K}(\mathbf{X}, \mathbf{X}) + \lambda \mathbf{I})^{-1} \right\|_2 \cdot \|\mathbf{y}\|_2 \\
&= \sqrt{n} \cdot \left\| \begin{bmatrix} \frac{\partial k(\mathbf{x}^*, \mathbf{x}_1)}{\partial \mathbf{x}^*} & \frac{\partial k(\mathbf{x}^*, \mathbf{x}_2)}{\partial \mathbf{x}^*} & \dots & \frac{\partial k(\mathbf{x}^*, \mathbf{x}_n)}{\partial \mathbf{x}^*} \end{bmatrix} \right\|_1 \\
&\quad \cdot \left\| (\mathbf{K}(\mathbf{X}, \mathbf{X}) + \lambda \mathbf{I})^{-1} \right\|_2 \cdot \|\mathbf{y}\|_2 \\
&= \sqrt{n} \cdot \max_{\mathbf{x}_i \in \mathbf{X}} \left\| \frac{\partial k(\mathbf{x}^*, \mathbf{x}_i)}{\partial \mathbf{x}^*} \right\|_1 \cdot \left\| (\mathbf{K}(\mathbf{X}, \mathbf{X}) + \lambda \mathbf{I})^{-1} \right\|_2 \cdot \|\mathbf{y}\|_2 \\
&\stackrel{(a)}{=} \sqrt{n} \cdot \max_{\mathbf{x}_i \in \mathbf{X}} \left\| \frac{\partial k(\mathbf{x}_i + \mathbf{d}_i, \mathbf{x}_i)}{\partial \mathbf{d}_i} \right\|_1 \cdot \left\| (\mathbf{K}(\mathbf{X}, \mathbf{X}) + \lambda \mathbf{I})^{-1} \right\|_2 \cdot \|\mathbf{y}\|_2,
\end{aligned}$$

where in (a), we used the chain rule together with  $\frac{\partial \mathbf{d}_i}{\partial \mathbf{x}^*} = \mathbf{I}$ .  $\square$

*Proof of Proposition 3.*

In spherical coordinates,

$$\left\| \frac{\partial k_G(\mathbf{d}_i, \sigma)}{\partial \mathbf{d}_i} \right\|_1 = \left| \frac{\partial k_G(\mathbf{d}_i, \sigma)}{\partial d_i} \right| + \sum_{j=2}^p \left| \frac{1}{d_i} \frac{\partial k_G(\mathbf{d}_i, \sigma)}{\partial \theta_j} \right|,$$

where the sum is over the angular coordinates. Since the Gaussian kernel is rotationally invariant, this sum is 0 and

$$\left\| \frac{\partial k_G(\mathbf{d}_i, \sigma)}{\partial \mathbf{d}_i} \right\|_1 = \left| \frac{\partial}{\partial d_i} \exp \left( -\frac{d_i^2}{2\sigma^2} \right) \right| = \frac{d_i}{\sigma^2} \exp \left( -\frac{d_i^2}{2\sigma^2} \right).$$

To find the  $d_i$  that maximizes the derivative, we look where the second derivative is zero.

$$\frac{\partial}{\partial d_i} \left| \frac{\partial k_G(d_i, \sigma)}{\partial d_i} \right| = \left( \left( \frac{d_i}{\sigma^2} \right)^2 - \frac{1}{\sigma^2} \right) \exp \left( -\frac{d_i^2}{2\sigma^2} \right).$$

Setting the second derivative to zero amounts to

$$\left( \frac{d_i}{\sigma^2} \right)^2 = \frac{1}{\sigma^2} \iff d_i^2 = \sigma^2 \implies d_i = \sigma.$$

Plugging this into the first derivative we obtain  $\frac{1}{\sigma} \exp \left( -\frac{1}{2} \right)$ , which is greater than

$$\left| \frac{\partial k_G(0, \sigma)}{\partial d_i} \right| = \left| \frac{\partial k_G(\infty, \sigma)}{\partial d_i} \right| = 0,$$

and consequently

$$\max_{\mathbf{d}_i} \left\| \frac{\partial k_G(\mathbf{d}_i, \sigma)}{\partial \mathbf{d}_i} \right\|_1 = \max_{d_i} \left| \frac{\partial k_G(d_i, \sigma)}{\partial d_i} \right| = \frac{1}{\sigma \sqrt{e}}.$$

$\square$

*Proof of Proposition 4.*

To alleviate notation, from now on we do not explicitly state that  $\mathbf{K}$  depends on  $\mathbf{X}$ . We first note that  $\left\| (\mathbf{K} + \lambda \mathbf{I})^{-1} \right\|_2 = \frac{1}{s_n(\mathbf{K} + \lambda \mathbf{I})}$ , where  $s_n$  denotes the smallest singular value of  $\mathbf{K}$ . Since  $\mathbf{K}$  is symmetric and positive semi-definite, it is

diagonalizable as  $\mathbf{K} = \mathbf{U}\mathbf{\Sigma}\mathbf{U}^\top$ , while  $\lambda\mathbf{I} = \lambda\mathbf{U}\mathbf{U}^\top$ , which means that  $\mathbf{K} + \lambda\mathbf{I} = \mathbf{U}(\mathbf{\Sigma} + \lambda\mathbf{I})\mathbf{U}^\top$ , i.e. the singular values of  $\mathbf{K} + \lambda\mathbf{I}$  are the singular values of  $\mathbf{K}$ , shifted by  $\lambda$ .

According to Bermanis et al. (2013), for  $\mathbf{x} \in \mathbb{R}^p$ , where each  $x_i$  is restricted to an interval of length  $l_i$ ,  $i = 1, 2, \dots, p$ , for a Gaussian kernel matrix  $\mathbf{K} \in \mathbb{R}^{m \times n}$ , with singular values  $s_1, \dots, s_n$ , the number of singular values larger than  $\delta \cdot s_1$  for some  $\delta > 0$ ,  $R_\delta(\mathbf{K})$ , is bounded according to

$$\begin{aligned} R_\delta(\mathbf{K}) &:= \# \left\{ j : \frac{s_j(\mathbf{K})}{s_1(\mathbf{K})} \geq \delta \right\} \leq \prod_{i=1}^d \left( \frac{2}{\pi} \frac{l_i}{\sigma} \sqrt{\log(1/\delta)} + 1 \right) \\ &\leq \left( \frac{2}{\pi} \frac{l_{\max}}{\sigma} \sqrt{\log(1/\delta)} + 1 \right)^p. \end{aligned}$$

Solving for  $\delta$ , we obtain

$$\begin{aligned} R_\delta(\mathbf{K}) &\leq \left( \frac{2}{\pi} \frac{l_{\max}}{\sigma} \sqrt{\log(1/\delta)} + 1 \right)^p \\ \iff (R_\delta(\mathbf{K})^{1/p} - 1) \frac{\pi\sigma}{2l_{\max}} &\leq \sqrt{\log(1/\delta)} \\ \iff \delta &\leq \exp \left( - \left( \frac{(R_\delta(\mathbf{K})^{1/p} - 1)\pi\sigma}{2l_{\max}} \right)^2 \right). \end{aligned}$$

Now, if  $R_\delta(\mathbf{K}) = n$ , then all singular values (including  $s_n$ ) are larger than or equal to  $\delta \cdot s_1$ . If  $R_\delta(\mathbf{K}) = n - 1$ , then all but one (namely  $s_n$ ) of the singular values are larger than or equal to  $\delta \cdot s_1$ . So for  $R_\delta(\mathbf{K}) = n - 1$ ,  $s_n < \delta \cdot s_1$ , which implies

$$\begin{aligned} s_n &< s_1 \delta \leq s_1 \exp \left( - \left( \frac{((n-1)^{1/p} - 1)\pi\sigma}{2l_{\max}} \right)^2 \right) \\ &\leq n \exp \left( - \left( \frac{((n-1)^{1/p} - 1)\pi\sigma}{2l_{\max}} \right)^2 \right), \end{aligned}$$

where we used  $s_1(\mathbf{K}) \leq n \cdot \|\mathbf{K}\|_{\max} = n \cdot 1$ .

Thus

$$\left\| (\mathbf{K} + \lambda\mathbf{I})^{-1} \right\|_2 = \frac{1}{s_n + \lambda} \geq \frac{1}{n \exp \left( - \left( \frac{((n-1)^{1/p} - 1)\pi\sigma}{2l_{\max}} \right)^2 \right) + \lambda}.$$

□

## References

- Ali, M., Prasad, R., Xiang, Y., and Yaseen, Z. M. (2020). Complete ensemble empirical mode decomposition hybridized with random forest and kernel ridge regression model for monthly rainfall forecasts. *Journal of Hydrology*, 584:124647.
- Amini, A. A. (2021). Spectrally-truncated kernel ridge regression and its free lunch. *Electronic Journal of Statistics*, 15(2):3743–3761.
- Bai, S., Koltun, V., and Kolter, J. Z. (2021). Stabilizing equilibrium models by jacobian regularization. *arXiv preprint arXiv:2106.14342*.
- Belkin, M., Ma, S., and Mandal, S. (2018). To understand deep learning we need to understand kernel learning. In *International Conference on Machine Learning*, pages 541–549. PMLR.
- Bermanis, A., Averbuch, A., and Coifman, R. R. (2013). Multiscale data sampling and function extension. *Applied and Computational Harmonic Analysis*, 34(1):15–29.
- Candanedo, L. M., Feldheim, V., and Deramaix, D. (2017). Data driven prediction models of energy use of appliances in a low-energy house. *Energy and Buildings*, 140:81–97.
- Chan, A., Tay, Y., Ong, Y. S., and Fu, J. (2019). Jacobian adversarially regularized networks for robustness. *arXiv preprint arXiv:1912.10185*.
- Chen, H. and Leclair, J. (2021). Optimizing etching process recipe based on kernel ridge regression. *Journal of Manufacturing Processes*, 61:454–460.
- Chen, L. and Xu, S. (2020). Deep neural tangent kernel and laplace kernel have the same rkhs. *arXiv preprint arXiv:2009.10683*.
- Chen, Z., Hu, J., Qiu, X., and Jiang, W. (2022). Kernel ridge regression-based tv regularization for motion correction of dynamic mri. *Signal Processing*, 197:108559.
- Cleveland, W. S. and Devlin, S. J. (1988). Locally weighted regression: an approach to regression analysis by local fitting. *Journal of the American statistical association*, 83(403):596–610.
- Fan, J. and Gijbels, I. (1995). Data-driven bandwidth selection in local polynomial fitting: variable bandwidth and spatial adaptation. *Journal of the Royal Statistical Society: Series B (Methodological)*, 57(2):371–394.
- Fan, P., Deng, R., Qiu, J., Zhao, Z., and Wu, S. (2021). Well logging curve reconstruction based on kernel ridge regression. *Arabian Journal of Geosciences*, 14(16):1–10.
- Finlay, C., Jacobsen, J.-H., Nurbekyan, L., and Oberman, A. (2020). How to train your neural ode: the world of jacobian and kinetic regularization. In *International conference on machine learning*, pages 3154–3164. PMLR.
- Geifman, A., Yadav, A., Kasten, Y., Galun, M., Jacobs, D., and Ronen, B. (2020). On the similarity between the laplace and neural tangent kernels. *Advances in Neural Information Processing Systems*, 33:1451–1461.
- Ghorbani, B., Mei, S., Misiakiewicz, T., and Montanari, A. (2020). When do neural networks outperform kernel methods? *Advances in Neural Information Processing Systems*, 33:14820–14830.
- Ghorbani, B., Mei, S., Misiakiewicz, T., and Montanari, A. (2021). Linearized two-layers neural networks in high dimension. *The Annals of Statistics*, 49(2):1029–1054.
- Hastie, T., Montanari, A., Rosset, S., and Tibshirani, R. J. (2022). Surprises in high-dimensional ridgeless least squares interpolation. *The Annals of Statistics*, 50(2):949–986.
- Hoffman, J., Roberts, D. A., and Yaida, S. (2019). Robust learning with jacobian regularization. *arXiv preprint arXiv:1908.02729*.
- Jacot, A., Gabriel, F., and Hongler, C. (2018). Neural tangent kernel: Convergence and generalization in neural networks. *Advances in neural information processing systems*, 31.
- Jakubovitz, D. and Giryes, R. (2018). Improving dnn robustness to adversarial attacks using jacobian regularization. In *Proceedings of the European Conference on Computer Vision (ECCV)*, pages 514–529.
- Köhler, M., Schindler, A., and Sperlich, S. (2014). A review and comparison of bandwidth selection methods for kernel regression. *International Statistical Review*, 82(2):243–274.
- Krige, D. G. (1951). A statistical approach to some basic mine valuation problems on the witwatersrand. *Journal of the Southern African Institute of Mining and Metallurgy*, 52(6):119–139.
- Le, Y., Jin, S., Zhang, H., Shi, W., and Yao, H. (2021). Fingerprinting indoor positioning method based on kernel ridge regression with feature reduction. *Wireless Communications and Mobile Computing*, 2021.

- Matheron, G. (1963). Principles of geostatistics. *Economic geology*, 58(8):1246–1266.
- Mei, S., Misiakiewicz, T., and Montanari, A. (2021). Generalization error of random feature and kernel methods: hypercontractivity and kernel matrix concentration. *Applied and Computational Harmonic Analysis*.
- Nadaraya, E. A. (1964). On estimating regression. *Theory of Probability & Its Applications*, 9(1):141–142.
- Pace, R. K. and Barry, R. (1997). Sparse spatial autoregressions. *Statistics & Probability Letters*, 33(3):291–297.
- Park, B. U. and Marron, J. S. (1990). Comparison of data-driven bandwidth selectors. *Journal of the American Statistical Association*, 85(409):66–72.
- Poggio, T., Kur, G., and Banburski, A. (2019). Double descent in the condition number. *arXiv preprint arXiv:1912.06190*.
- Safari, M. J. S. and Rahimzadeh Arashloo, S. (2021). Kernel ridge regression model for sediment transport in open channel flow. *Neural Computing and Applications*, 33(17):11255–11271.
- Shahsavari, A., Jamei, M., and Karbasi, M. (2021). Experimental evaluation and development of predictive models for rheological behavior of aqueous  $\text{Fe}_3\text{O}_4$  ferrofluid in the presence of an external magnetic field by introducing a novel grid optimization based-kernel ridge regression supported by sensitivity analysis. *Powder Technology*, 393:1–11.
- Sheather, S. J. and Jones, M. C. (1991). A reliable data-based bandwidth selection method for kernel density estimation. *Journal of the Royal Statistical Society: Series B (Methodological)*, 53(3):683–690.
- Silverman, B. W. (2018). *Density estimation for statistics and data analysis*. Routledge, .
- Singh Alvarado, J., Goffinet, J., Michael, V., Liberti, W., Hatfield, J., Gardner, T., Pearson, J., and Mooney, R. (2021). Neural dynamics underlying birdsong practice and performance. *Nature*, 599(7886):635–639.
- Vanwysberghe, C. (2021). Kriging the french temperatures. <https://towardsdatascience.com/kriging-the-french-temperatures-f0389ca908dd>.
- Watson, G. S. (1964). Smooth regression analysis. *Sankhyā: The Indian Journal of Statistics, Series A*, pages 359–372.
- Williams, C. K. and Rasmussen, C. E. (2006). *Gaussian processes for machine learning*. MIT press Cambridge, MA, .
- Wood, S. N., Li, Z., Shaddick, G., and Augustin, N. H. (2017). Generalized additive models for gigadata: Modeling the uk black smoke network daily data. *Journal of the American Statistical Association*, 112(519):1199–1210.
- Wu, Y., Prezhdo, N., and Chu, W. (2021). Increasing efficiency of nonadiabatic molecular dynamics by hamiltonian interpolation with kernel ridge regression. *The Journal of Physical Chemistry A*, 125(41):9191–9200.
- Zahrt, A. F., Henle, J. J., Rose, B. T., Wang, Y., Darrow, W. T., and Denmark, S. E. (2019). Prediction of higher-selectivity catalysts by computer-driven workflow and machine learning. *Science*, 363(6424):eaau5631.